Wear 271 (2011) 1445–1453

Contents lists available at ScienceDirect

Wear

journal homepage: www.elsevier.com/locate/wear

Cavitation erosion of martensitic and austenitic stainless steel welded coatings

J.F. Santa[a,b,*], J.A. Blanco[a,b], J.E. Giraldo[b], A. Toro[a]

[a] Tribology and Surfaces Group, National University of Colombia, Cra 80 No. 65-223, Medellín, Colombia
[b] Welding Group, National University of Colombia, Cl59A No. 63-20, Medellín, Colombia

ARTICLE INFO

Article history:
Received 16 September 2010
Received in revised form
22 December 2010
Accepted 23 December 2010

Keywords:
Cavitation erosion resistance
Welded coatings
Stainless steels
Microstructure
Wear mechanisms

ABSTRACT

The cavitation erosion resistance of four alloys used to repair worn turbines by welding was tested in laboratory. AWS E309 alloy (3 layers) and a High-Cobalt stainless steel (2 and 3 layers) were applied by manual process (SMAW) onto ASTM A743 grade CA6NM stainless steel (commonly known as 13-4 steel) and their cavitation resistance was compared to that of conventional alloys E410NiMo (applied by SMAW) and a ER410NiMo (applied by semiautomatic process GMAW). The microstructure of the weld deposits was studied by Light Optical Microscopy (LOM), Scanning Electron Microscopy (SEM) and X-Ray Diffraction (XRD), while the chemical composition was analyzed by Optical Emission (OES) and Energy Dispersive X-Ray Spectrometry (EDXS). Cavitation erosion tests were performed in an ultrasonic tester according to ASTM G32 standard and the worn surfaces were analyzed by SEM and XRD. The best cavitation erosion resistance of all the materials tested was shown by the High-Cobalt stainless steel coating applied in 3 layers, while the AWS E309 presented the highest value of maximum erosion rate. Conventional E410NiMo and ER410NiMo alloys showed an intermediate behavior. Incubation periods were 10.9 h and 21.5 h for High-Cobalt stainless steel in 2 and 3 layers, respectively, and 1.4 h for the 13-4 steel. In High-Cobalt stainless steel samples, occurrence of austenite-to-martensite phase transformation and profuse formation of twins and slip lines at the worn surfaces were observed.

1. Introduction

Cavitation erosion is the mechanical degradation of a surface as a consequence of continuous collapse of cavities or bubbles in a surrounding liquid, which seriously affects the operation of hydraulic equipment such as hydroelectric turbines, valves, fittings, pumps, ship propellers, among others. When cavitation occurs, erosion is caused by extremely concentrated mechanical loads that lead to plastic deformation at the solid surfaces.

In the case of hydro-turbines, cavitation erosion promotes formation of cavities or pits at the surface and modifies the hydraulic profile of the components, as can be seen in Fig. 1. Given that the efficiency of a turbine is highly dependent on its hydraulic profile, any change in the geometry associated with cavitation leads to significant mass losses of the component. Regarding Pelton turbines specifically, three regions of the buckets are very sensitive to cavitation erosion: the splitter (Fig. 1c), the tip (Fig. 1d) and the inner region marked as II in Fig. 1a. When wear exceeds certain limits in those areas the turbine must be repaired in order to maintain the efficiency of power generation within acceptable values.

Traditionally, field repairs have been carried out by welding with martensitic stainless steel fillers with the same chemical composition of the base metals. However, those alloys do not improve significantly the cavitation erosion resistance of the turbine and therefore the build-up procedures must be carried out frequently. This situation leads to high maintenance costs and reduces the profits of hydroelectric power plants since their operation is strongly based on the availability of the power units. Moreover, the welding reparations are time-consuming and require experienced operators to carry out the grinding procedures given that the hydraulic profile is the most important aspect of the turbine [1].

Some well-known cavitation resistant materials such as Co-based alloys Stellite 6 and Stellite 21 [2] usually exhibit relatively high hardness and corrosion resistance, and. However, these alloys are crack sensitive, difficult to grind and very expensive [3,4]. On the other hand, High-Cobalt stainless steels have been recognized for their high cavitation erosion resistance and they are considered as an alternative to Co-based alloys [3]. Furthermore, High-Cobalt stainless steels exhibit a strain-induced austenite-to-ε-martensite transformation which has been associated with their high cavitation erosion resistance [2].

Commercial High-Cobalt stainless steels were developed by the end of the 1980s [3] and since then they are available in the market in the form of welding wires and sticks. Although those base alloys have been developed and modified by diverse manufacturers over the years, their performance in terms of cavitation erosion resis-

* Corresponding author.
E-mail address: jfsanta@gmail.com (J.F. Santa).

0043-1648/$ – see front matter © 2011 Elsevier B.V. All rights reserved.
doi:10.1016/j.wear.2010.12.081

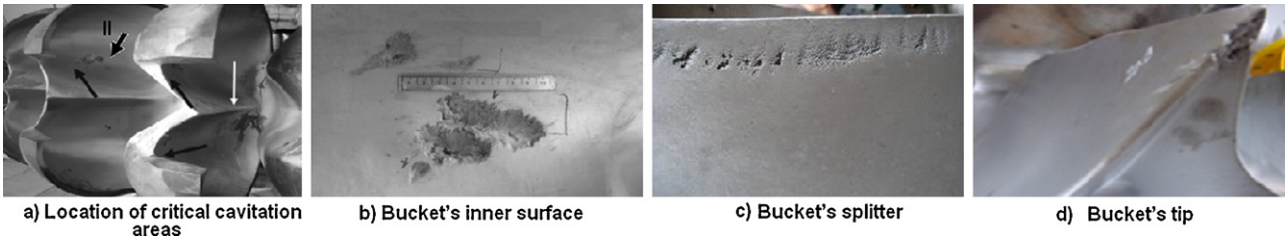

Fig. 1. (a–d) Typical cavitation erosion marks in a Pelton turbine.

tance has not been fully understood yet. Most articles in literature cite High-Cobalt alloys only as reference materials [5–7] but no profound discussion of their wear mechanisms is regularly found. In addition to that, in many cases the comparison with other materials is done based only in terms of erosion rate obtained from the cavitation erosion curve [5,6]. The incubation period and the precise correlations between wear mechanisms and microstructure, as well as the know-how of the welding procedures are still uncertain to some extent, and usually a great deal of technical support from the companies is required by the average user.

In this work, the microstructure and cavitation resistance of a number of welded coatings with potential application to repair worn turbine components were studied in laboratory. The results were compared to those obtained with two stainless steels commonly used for manufacturing hydraulic turbines.

2. Experimental procedure

2.1. Materials and welding procedure

Welded coatings obtained with four different commercial filler metals used to repair hydraulic turbines were studied, namely martensitic AWS E410NiMo (SMAW Process) and AWS ER410NiMo alloys (GMAW Process), austenitic AWS E309 stainless steel and High-Cobalt stainless steel (HCo from now on). Two martensitic stainless steels commonly used for manufacturing Pelton turbines, i.e. ASTM A743 grade CA6NM (from now on, 13-4 steel) and ASTM A743 grade CA15 (from now on, 13-1 steel) were used as comparison materials. The chemical composition obtained by Optical Emission Spectrometry (OES) and Energy dispersive X-Ray spectrometry (EDXS-SEM) of the tested materials is shown in Table 1. All the measurements were performed at the surfaces intended to be exposed to cavitation during the tests described in Section 2.3.

The welded coatings of E410NiMo, AWS E 309 and HCo were applied onto 13-4 steel coupons (Fig. 2) by SMAW process following different welding procedures whose details are shown in Table 2, although in all cases the test samples were preheated at 100 °C. Two and three weld layers were applied onto the same welding coupons, which were then properly cut as shown in Fig. 2 in order to extract the samples for cavitation erosion tests and microstructure evaluation taking care of discarding the ends to avoid discontinuities associated with starts and stops of passes, such as pores and slag entrapment. The samples were machined with adequate control of the depth of cut in order to obtain flat testing surfaces with

Table 1
Chemical composition of the studied materials (wt%). Measurements carried out by OES unless otherwise specified.

Material	C	Si	Mn	S	P	Ni	Cr	Mo	Cu	V	Co
13-4 Steel[a]	0.05	0.80	0.69	0.002	0.010	3.78	12.73	0.52	0.45	0.02	0.01
13-1 Steel[a]	0.037	0.436	0.706	0.009	0.018	1.801	12.51	–	–	0.030	–
E410 NiMo[b]	0.032	0.464	0.660	0.002	0.020	4.556	13.05	0.286	0.027	0.046	–
ER410 NiMo[b]	0.033	0.489	0.726	0.004	0.021	4.490	12.55	0.558	0.084	0.034	–
AWS E 309	0.048	0.531	1.258	0.011	0.029	11.796	22.042	0.045	0.22	0.087	–
HCo-2 layers[c]	–	2.1	7.6	–	–	0.9	16.4	–	–	–	7.2
HCo-3 layers[c]	–	2.3	9.5	–	–	0.4	16.5	–	–	–	8.2

[a] Base metals.
[b] E 410 NiMo and ER 410 NiMo have similar chemical compositions but the former is intended to be applied by SMAW process while the latter is applied by GMAW process.
[c] Measurements carried out by EDXS-SEM.

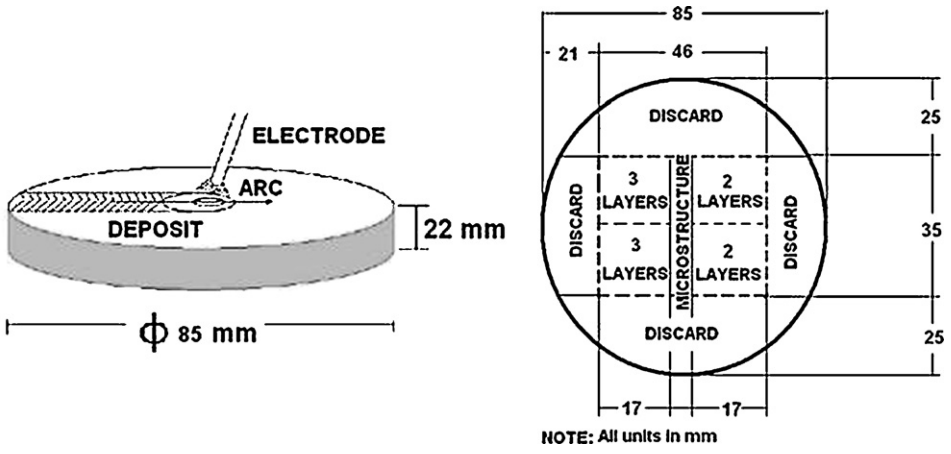

Fig. 2. Coatings deposition setup and sampling scheme.

Table 2
Processing parameters used during deposition of coatings by welding.

Coating	Process	Diameter/mm	Current/A	Voltage/V	Welding speed/$\times 10^{-3}$ m s^{-1} (ipm[a])
AWS E 309	SMAW	3.2	90	–	3.8 (9)
HCo alloy	SMAW	3.2	130	25–30	3.8 (9)
E410NiMo	SMAW	3.2	100	–	3.8 (9)
ER410NiMo	GMAW	1.1	250	34	5.9 (14)

SMAW: shielded metal arc welding; GMAW: gas metal arc welding.
[a] Inches per minute.

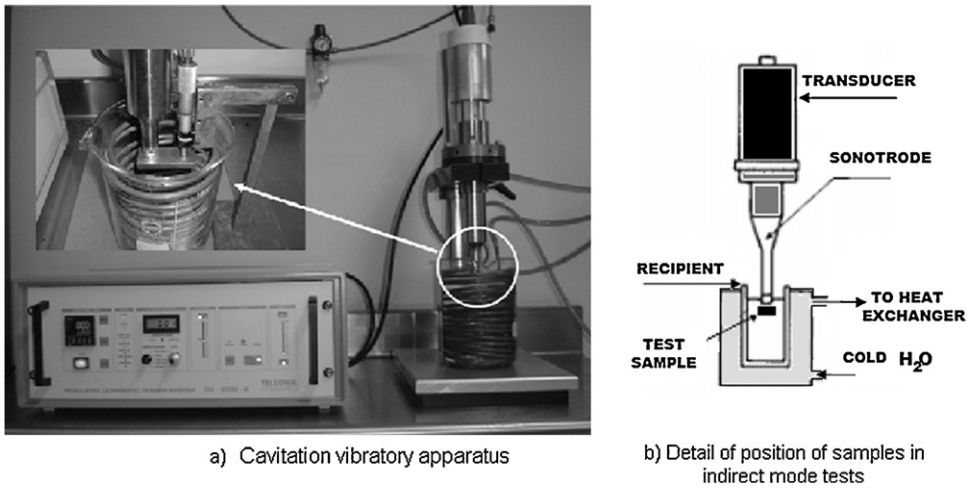

Fig. 3. (a–d) Cavitation vibratory apparatus operating in indirect mode.

similar thickness reductions. The thicknesses of the two and three-layer coatings were 3.5 mm and 5 mm, respectively. On the other hand, ER410NiMo cavitation test samples were extracted from a welded coupon used to perform a filler metal qualification procedure according to ASME IX, 2007 [8].

Regarding the comparison materials, the test samples of 13-1 steel were extracted from a bucket of a worn Pelton turbine, while 13-4 steel test samples were taken from cast bars manufactured by Villares metals, São Paulo, Brazil, homogenized at 1050 °C for 1 h, air-cooled to room temperature and then tempered at 620 °C for 1 h and cooled down in air.

2.2. Microstructure and chemical characterization

The microstructure characterization of the studied materials was done in a Nikon PME3 Light Optical Microscope (LOM) and in a JEOL 5910LV Scanning Electron Microscope (SEM). Microanalyses of the specimens were carried out in an Energy Dispersive X-Ray Spectrometer (EDXS) coupled to the SEM. Vickers hardness and micro-hardness measurements were performed by using a Wolpert hardness tester (HV62.5 kgf) and a Shimadzu micro-hardness tester (HV500 g, 15 s), respectively. The samples were ground with emery papers, polished using 1 μm diamond paste and then electrolytically etched in 10% oxalic acid at 5 V for 45 s.

2.3. Cavitation erosion tests

The cavitation erosion resistance of the studied materials was evaluated by ultrasonic vibratory tests according to ASTM G32 standard (Fig. 3) using a tip of stainless steel submerged in distilled water under the testing conditions presented in Table 3. The tests were of indirect-type, where the sample is not attached to the tip of the vibrating horn but fixed in front of it, at a distance of 500 μm.

The initial roughness of the samples was fixed to around Ra = 0.08 μm and Rq = 0.11 μm and the surface changes were monitored every hour during the tests by using a Mitutoyo SJ-210 stylus profilometer operating with a cut-off length of 0.8 mm and a total evaluation length of 4.8 mm. The mass losses were also registered every hour by using a scale with a resolving power of 0.01 mg and hardness measurements with different loads (at least five on each sample) were carried out at the beginning and at the end of the tests. Each test lasted for at least 6 h and at least two replicas of each material were analyzed.

After the tests, the eroded surfaces were observed by SEM and, in some cases, X-Ray Diffraction analyses were also performed in order to investigate the microstructure changes near to the worn surface. An X'Pert Pro diffractometer with Cu Kα radiation and 2-D PixCEL detector was used and the results were analyzed using X'Pert High Score Plus software with PDF2-2006 database.

Following ASTM G32 standard, the incubation time was calculated as the intercept on the testing time axis of a straight line extension of the maximum-slope portion of the cumulative erosion-time curve. Accordingly, the slope of such straight line (once the first stable maximum rate was observed) was reported as the maximum erosion rate during the tests.

3. Results and discussion

3.1. Microstructure

The microstructure of the welded coatings and stainless steels is shown in Fig. 4. 13-1 steel (Fig. 4a) is composed of tem-

Table 3
Testing parameters in cavitation erosion tests.

Frequency	20 ± 0.2 kHz
Amplitude	50 ± 2.5 μm
Fluid	Distilled water
Temperature	22 ± 1 °C
Mass loss measurements	Cleaning, drying and weighing every hour
Total testing time	At least 6 h

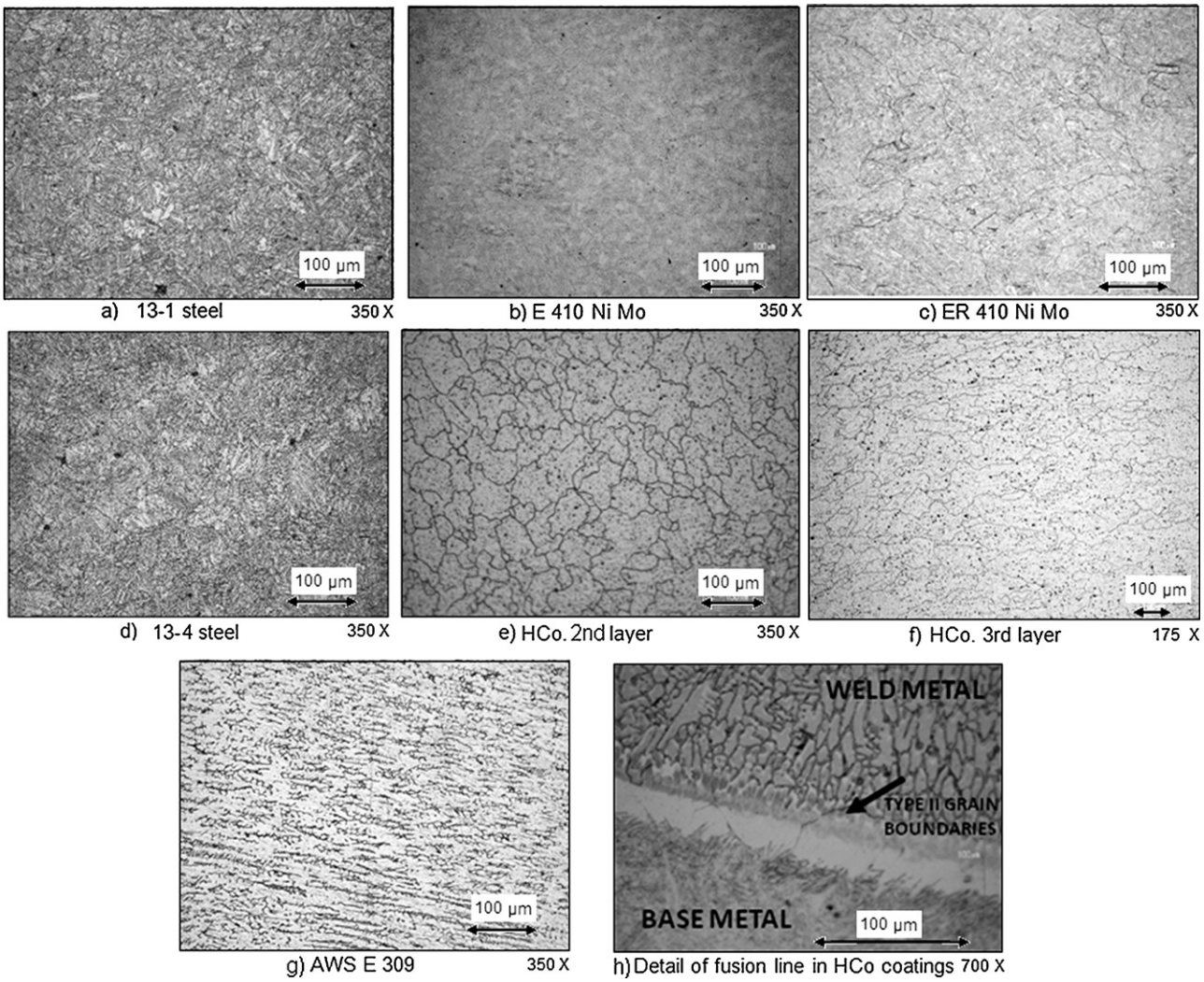

Fig. 4. (a–f) Microstructure of welded coatings and stainless steels.

pered martensite (ferrite and carbides) with average hardness of 227 ± 2 HV, while 13-4 steel (Fig. 4d) has an average hardness of 284 ± 6 HV and a microstructure composed of martensite, delta ferrite and retained austenite. E410NiMo (Fig. 4b) and ER410NiMo (Fig. 4c) coatings are also martensitic and have similar chemical compositions (Table 1), but their average hardness are different (409 ± 13 HV and 364 ± 22 HV, respectively) due to disparities in heat exchange rates during cooling for SMAW and GMAW processes. The microstructure of both 2-layer and 3-layer HCo coatings (Fig. 4e and f, respectively) is composed of austenite (278 ± 4 HV) and no other phases such as carbides or ferrite were identified. The microstructure of AWS E309 samples is composed of austenite and delta ferrite (Fig. 4g) as a result of its solidification sequence according to Schaffer diagram and its average hardness is 160 HV. In summary, the main differences among the studied stainless steels and welded coatings are the hardness of the martensitic phase and the presence or not of austenite and delta ferrite phases.

Some additional features of the microstructure of the coatings in relation with the fusion line are relevant having in mind that these alloys can be used to repair worn turbines. When a coating with a Face-Centered-Cubic (FCC) crystal structure (AWS E309 or HCo) is applied onto 13-4 steel which has a Body-Centered-Cubic (BCC) crystal structure at high temperature epitaxial growth does not take place at the interphase. Therefore, new grains must nucleate along the fusion line forming type II boundaries and making the material more vulnerable to failure by cracking under cyclic stresses, which is sometimes termed disbonding [9]. Moreover, in some cases a hard layer of martensite forms as a consequence of high cooling rates and diffusion of Carbon from the filler metal. In this work, type II grain boundaries were observed in HCo coatings as can be seen in Fig. 4h. EDXS measurements (Fig. 5) revealed abrupt variations of concentration of elements such as Mn, Ni, Co, Cr and Si over a distance of 50 µm from the fusion line. These variations in chemical composition are responsible for changes in the solidification behavior and could lead to the formation of martensite near the fusion line.

3.2. Cavitation erosion resistance

Fig. 6 shows the variation of cumulative mass loss as a function of testing time for all the studied samples (left) and a close-up view of the first 6 h of testing (right). It can be seen that austenitic HCo-3 layers samples showed the best behavior of all the materials tested. For instance, after a reference testing time of 6 h, the cumulative mass loss of HCo-3 layers samples was around 16 and 9 times lower than that of reference materials 13-4 and 13-1 steels, respectively. On the other hand, although austenitic AWS E309 exhibited the highest cumulative mass loss of all the tested materials, it can still be considered a good alternative to conventional filler metals in order to avoid excessive dilution on base metals

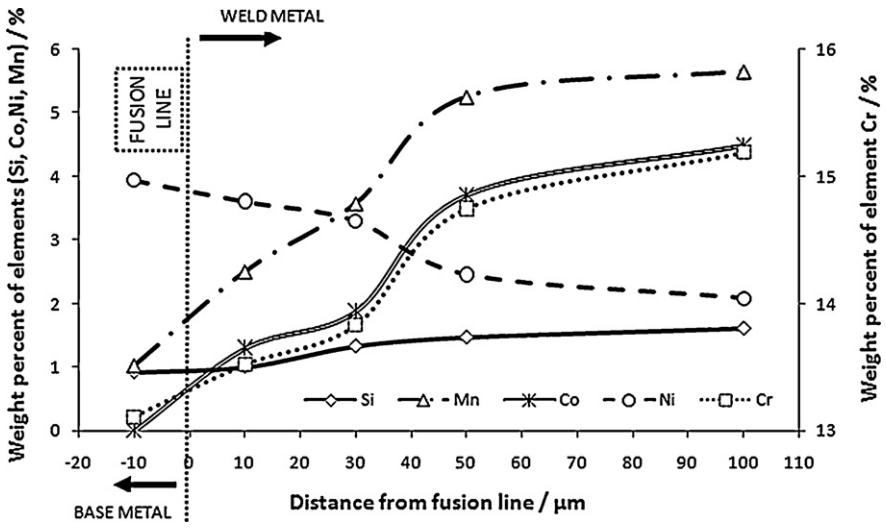

Fig. 5. Variation of alloy elements near the fusion line.

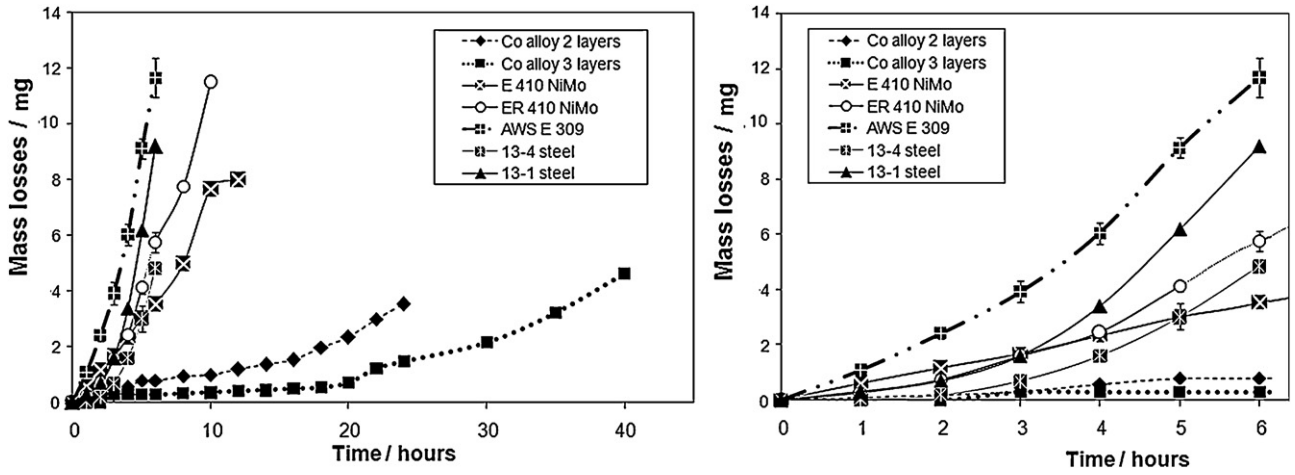

Fig. 6. Variation of cumulative mass loss with testing time.

and may be used as a butter layer [9] because of its high contents of Ni and Cr. Regarding the coatings with martensitic microstructure, E410NiMo showed slightly better cavitation resistance than ER410NiMo, being the mass losses of both materials comparable to that of 13-4 steel and lower than that of 13-1 steel. These results are in agreement with those found by Pereira [10].

With respect to the incubation stage (Fig. 7) the longest incubation period was found in HCo-3 layers (21.5 h) followed by HCo-2 layers (10.9 h), while the AWS E309 exhibited the shortest one (1.8 h). The martensitic coatings with 13 wt% Cr and 4 wt% Ni (13-4 steels, E410NiMo and ER410NiMo) showed similar incubation periods, in the order of 4–4.5 h.

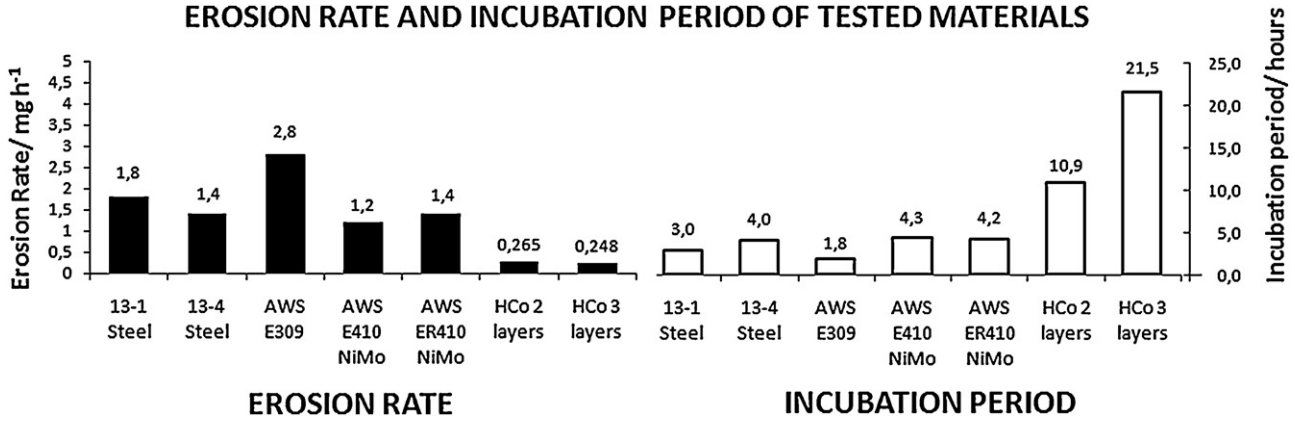

Fig. 7. Incubation period and maximum erosion rate reported during the test.

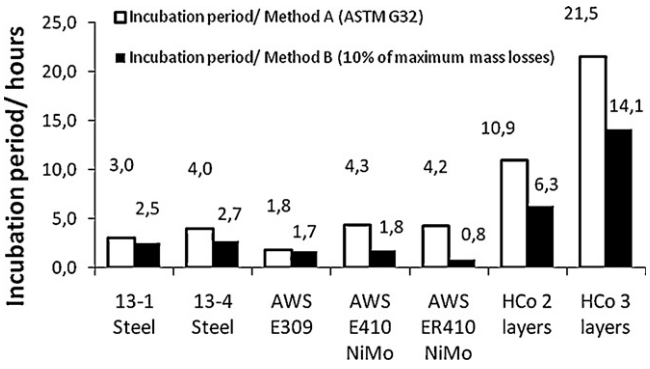

Fig. 8. Comparison of values of incubation period.

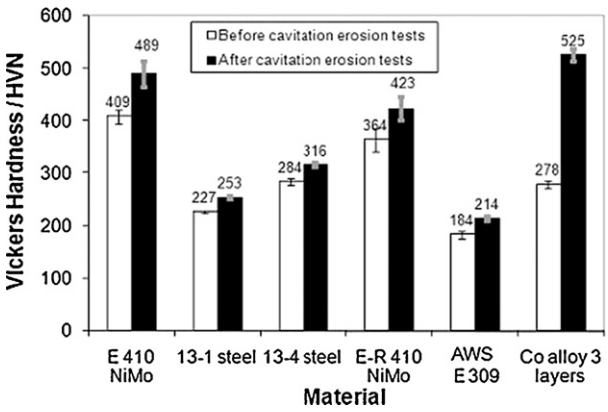

Fig. 9. Hardness of tested materials before and after the cavitation tests.

It is worth noticing at this point that the values of incubation time can strongly vary depending on the method employed to compute them. When the incubation time is calculated following ASTM G32 standard as the intercept on the testing time axis of a straight line extension of the maximum-slope portion of the cumulative erosion–time curve, the values tend to be greater than those expected from the direct observation of the curves of cumulative mass loss in Fig. 6. On the other hand, if according to a stricter criterion, only the portion of the test in which no mass loss occurs is considered, the obtained values are generally very low and in some cases could not be regarded as representative of the real response of the material. In this work, both approaches were contemplated and the mean values obtained for each material are shown in Fig. 7. To determine the incubation period following the "zero mass-loss" criterion an arbitrary offset was established, according to which any mass loss smaller than 10% of the maximum mass loss measured for each material during the test was considered negligible (Fig. 8).

Fig. 7 also shows the maximum erosion rate reported during the tests for all the samples, calculated from the time–variation cumulative mass curves presented in Fig. 6b. The highest values obtained for austenitic AWS E309 coating and reference material 13-1 steel are consistent with the significant surface damage observed in these samples, as will be discussed in detail in Section 3.4. On the other hand, HCo-2 and 3 layers showed a lower erosion rate which can be mainly associated to differences in chemical composition of the exposed surface (Table 1) as a result of dilution of the filler metal during the deposition process. A higher concentration of elements such Mn, Si and Co can reduce the stacking fault energy of the austenite [11] and consequently lead to longer incubation times [3,12,13] and lower erosion rates since the detachment of particles is delayed by energy dissipation.

Regarding the E410 NiMo and ER 410 NiMo martensitic coatings, the results showed that mass losses were higher than 13-4 stainless steel. It is noteworthy that the coatings were not heat treated, which is a common practice in the case of minor repairs in Pelton turbines. That fact led to higher hardness of the coatings (the initial values are reported in Fig. 9) compared with 13-4 steel, which, however, did not result in higher cavitation erosion resistance. This is important since it means that repairing worn components with the studied martensitic coatings will decrease the cavitation erosion resistance, i.e. a Pelton turbine would have to be repaired sooner when the coatings are applied and no heat treatment is performed afterwards.

3.3. Hardening effects

Fig. 9 shows that all the samples experienced an increase in hardness as a result of the cavitation experiments. This can be attributed mainly to strain hardening effects due to accumulation of plastic deformation beneath the surface, although the metastable austenite-to-martensite phase transformation is also expected to play an important role.

Fig. 10 shows the XRD patterns of austenitic HCo-3 layers and AWS E309 samples before and after the cavitation tests. Clear evidences of martensite formation in HCo-3 layers can be observed, which are consistent with the higher increments in hardness measured in this material. On the other hand, the XRD patterns for AWS E309 show no significant formation of martensite but a texture accommodation of austenite, represented in variations of the relative intensities of (1 1 1) and (2 0 0) peaks. The higher stability of austenite in AWS E309 could be attributed in part to the combined effects of the alloying elements on the thermodynamics and kinetics of martensitic transformation, since in this material the (Ni_{eq}/Cr_{eq}) ratio is (13.97/22.88 = 0.61), which is 32% greater than in HCo-3 layers (9.25/19.95 = 0.46).

With respect to the martensitic coatings, E410NiMo and ER410NiMo showed higher increases in hardness than 13-1 and 13-4 stainless steels, which are chemically comparable. This behavior could be related to the fact that the coatings are expected to have higher volume fractions of retained austenite as a consequence of the higher cooling rates generated during the welding processes [12]. However, the XRD patterns obtained were not conclusive since the detection of austenite in these steels requires the use of specialized techniques that were not utilized in this work [14].

3.4. Wear mechanisms and examination of worn surfaces

Fig. 11 illustrates the variation of roughness of the samples over a testing period of 6 h. HCo-2 and -3 layers showed no significant changes in Rq, which is consistent with the fact that these alloys presented incubation periods much longer than 6 h, so the expected deformation at their surface is still very small. The AWS E309 coating, on the other hand, had roughness variations comparable to those of reference 13-1 and 13-4 steels. The roughness changes in martensitic E410NiMo and ER410NiMo coatings were smaller than in reference 13-4 and 13-1 steels, but still significant with respect to the HCo samples.

Fig. 12 shows the aspect of the worn surfaces of tested coatings and stainless steels, as observed in stereomicroscope. The wear marks are surrounded by a slightly shaded ring, which is typically observed in samples submitted to stationary cavitation tests. According to García-Atance Fatjó [15] the ring is caused by differences in fluid movement around the horn due to periodical differences in kinematic energy on the radial direction of the tip.

The differences between the worn surfaces of conventional turbine materials and HCo steels are evident: the surfaces of 13-1 and 13-4 steels showed deep erosion marks while HCo steels presented only slightly shaded areas after the same testing time, and even

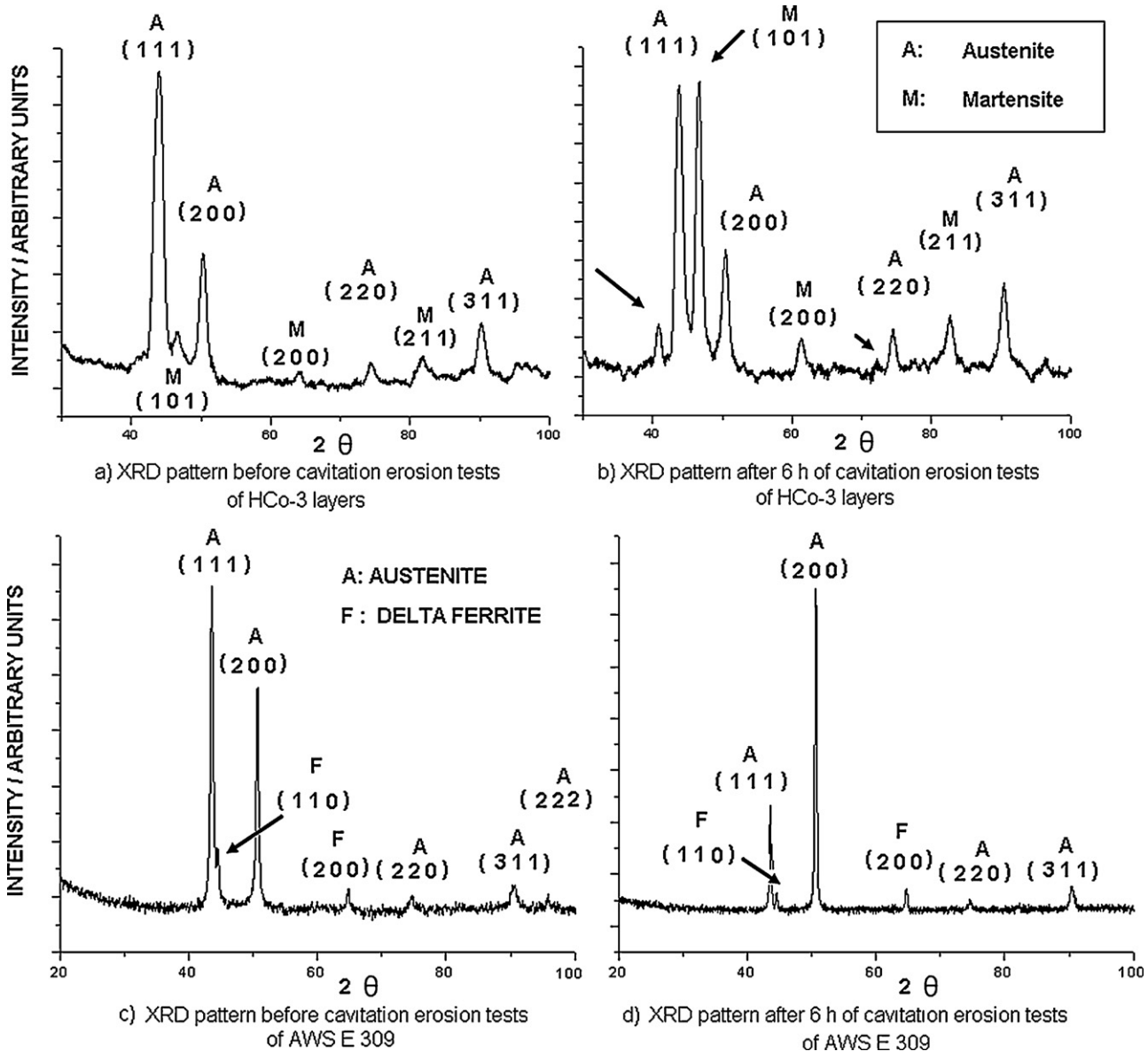

Fig. 10. (a–d) XRD patterns of HCo-3 layers and AWS E309 samples before and after the cavitation tests.

after longer exposures the surface of HCo-3 layers was still in better condition, as can be seen in Fig. 12g for a sample tested for 40 h. The examination of the surfaces also showed that plastic deformation was more significant in AWS E 309 than in 13-1 and 13-4 steels.

Fig. 13 shows the aspect of the worn surfaces as observed in SEM. The surfaces of the martensitic samples presented striations, which are typical of fatigue processes and accumulation of plastic deformation. The main mass removal mechanism was detaching of wear particles as a consequence of the coalescence of cracks that initiated in highly deformed regions.

In HCo steels, two processes of energy dissipation are expected to occur during cavitation tests [13]: in the first stage new stacking faults are formed and evidences of twinning and multiple slip can be seen (see the arrows in Fig. 13c); afterwards, formation of ε-martensite changes the wear mechanism due to the development of triangular structures that cause the detachment of plates by brittle fracture. This sequence leads to a distinctive microstructure composed by thin layers of fresh ε-martensite surrounded by tough austenite grains, which helps absorb the impact energy of the elastic waves in a very efficient way [13]. These processes of

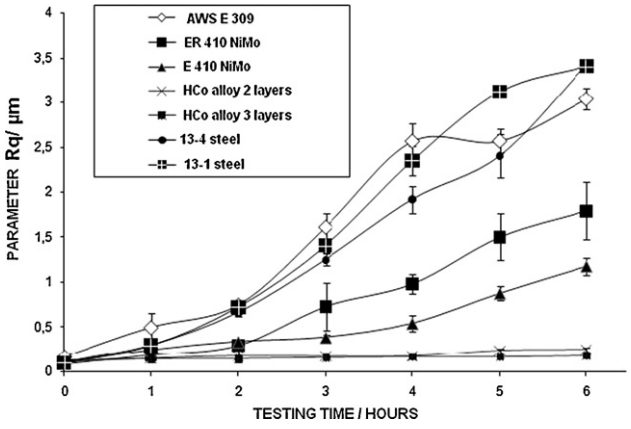

Fig. 11. Variation of roughness parameter Rq during cavitation tests.

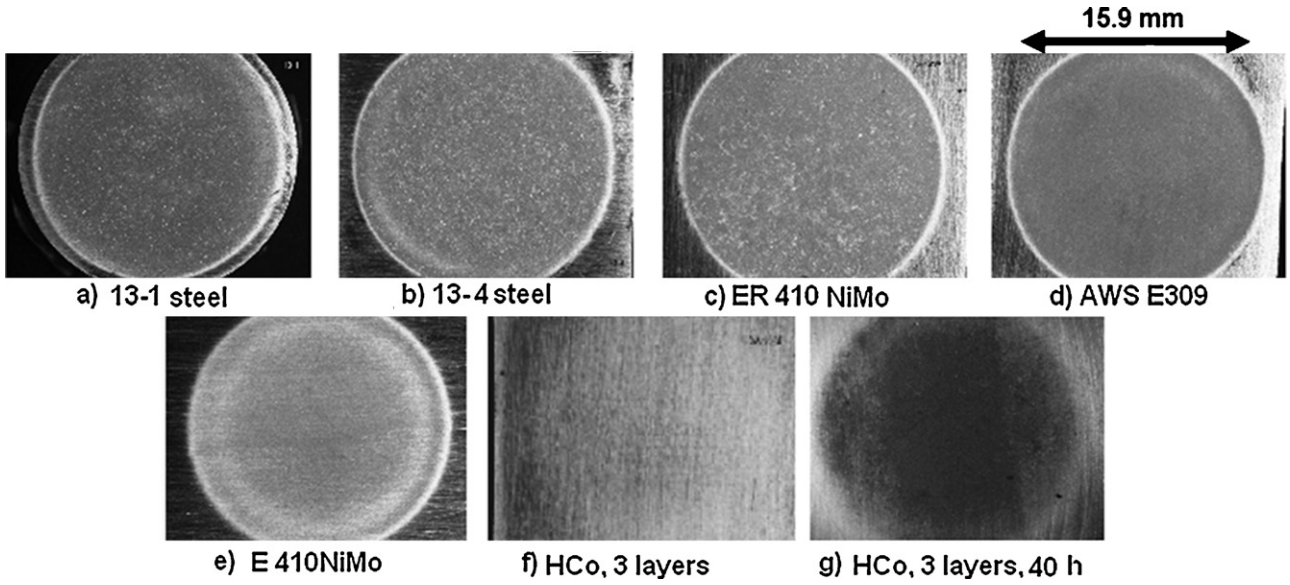

Fig. 12. (a–g) Worn surfaces of tested coatings and stainless steels.

energy dissipation led to higher incubation periods since the fatigue process and the beginning of detachment of small particles by accumulation of plastic deformation are delayed by the absorption of elastic waves through the creation of new lattice defects.

In martensitic coatings (ER 410 NiMo and E 410 NiMo), besides the expected high volumetric fraction of austenite, the elevated hardness causes the failure mechanism to be mostly fragile. The small islands in Fig. 13b showed evidences of microcracking, which was also observed in 13-4 and 13-1 steels albeit to a lesser degree. This brittle behavior is related to the fact that no post-weld heat treating (PWHT) was carried out after deposition of the coatings, which is frequently the case when hydraulic turbines are repaired in the field. Additionally, martensitic structures have more lattice defects and they do not dissipate energy as efficiently as austenitic structures do.

The high mass losses observed in AWS E309 samples can be related to the characteristics of the phases in the microstructure. Ferrite is the weakest phase of this material and is preferentially attacked, together the ferrite/austenite interphase. According to Stachoviak [16], the resistance to cavitation of ferrite is inferior to that of austenite while martensite has the best behavior. The high volume fraction of delta ferrite is not beneficial in cavitation erosion in spite of its advantages from the metallurgical point of view during the solidification of the alloy [17,18].

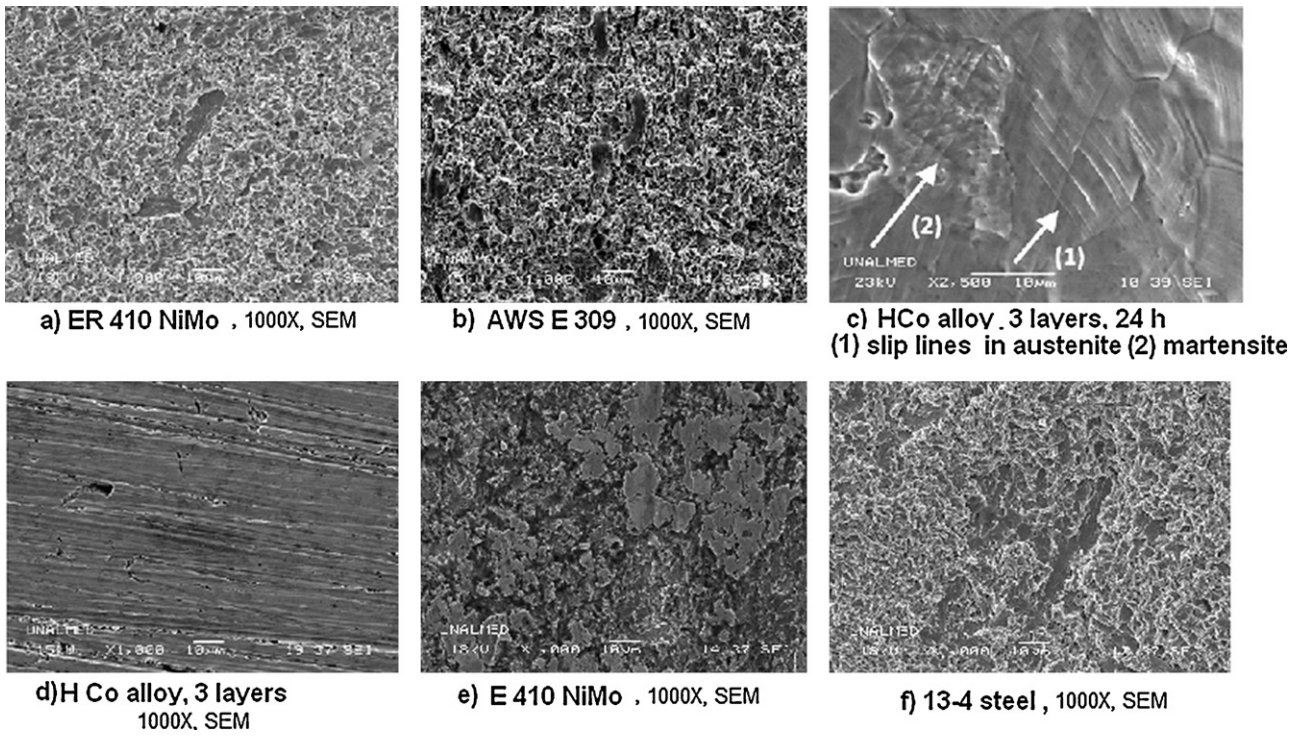

Fig. 13. (a–f) Worn surfaces of tested coatings and stainless steel as observed in SEM.

4. Conclusions

The cavitation erosion resistance of two martensitic coatings (E410NiMo, ER410NiMo) and two austenitic coatings (AWS E309, and HCo) was tested in laboratory in order to evaluate the suitability of these materials for welding repairs of worn hydraulic turbines. Conventional 13-1 and 13-4 stainless steels were also tested for comparison purposes. The main conclusions are as follows:

- HCo steels coatings showed the best cavitation erosion resistance of all the materials tested, being the incubation period the parameter more significantly improved with respect to uncoated stainless steels. The lowest wear resistance was observed in AWS E 309 coating and conventional 13-1stainless steel.
- E410NiMo and ER410NiMo martensitic coatings applied by welding did not exhibit significantly better cavitation erosion resistance when compared to conventional 13-4 steel.
- The main wear mechanisms observed in martensitic alloys were plastic deformation, fatigue and coalescence of cracks.
- In HCo alloys a particular damage sequence was observed, consisting of twinning followed by austenite-to-martensite transformation and subsequent mass removal form triangular structures, which were formed according to the crystallographic features of the phase transformation once the austenite transformed to martensite.

Acknowledgements

The authors thank to Empresas Públicas de Medellín for their technical support. Financial support provided by Colciencias-Empresas Públicas de Medellín-UNAL project no. 20201005975 is also acknowledged.

References

[1] S.C. Li, Cavitation of Hydraulic Machinery, Imperial College Press, 2000.
[2] S. Hattori, N. Mikamia, Cavitation erosion resistance of stellite alloy weld overlays, Wear 267 (October (11)) (2009) 1954–1960.
[3] D. Hart, D. Whale, A Review of Cavitation–Erosion Resistant Weld Surfacing Alloys for Hydroturbines, Eutectic Australia Pty Ltd., Sydney, Australia, 1999.
[4] J.H. Boy, A. Kumar, P. March, P. Willis, H. Herman, Cavitation and Erosion Resistant Thermal Spray Coatings, USACERL, Technical Report 97/118, USA, 1997.
[5] Performance of NOREM Hardfacing Alloys, EPRI, Palo Alto, CA, 1999, TR-112993.
[6] L. Boccanera, et al., Cavitation erosion resistance of Co-alloyed stainless steel weld claddings as compared to thermal sprayed coatings, in: Proceeding of: XXV Encontro nacional de tecnologia da soldagem, Belo Horizonte, Brazil, September 8–10 de 1999.
[7] A. Kumar, J. Boy, R. Zatorski, L.D. Stephenson, Thermal spray and weld repair alloys for the repair of cavitation damage in turbines and pumps: a technical note, Journal of Thermal Spray Technology 14 (June (2)) (2005) 177–182.
[8] ASME Boiler & Pressure Vessel Code, Section IX, 2007.
[9] J.C. Lippold, D.J. Kotecki, Welding Metallurgy and Weldability of stainless Steels, 2005.
[10] S.A. Pereira, Desenvolvimento de Procedimento de Reparo por Soldagem em Aços Inoxidáveis Martensíticos com Metal de Adição Similar sem TTP, Dissertação de Mestrado em Engenharia Mecânica, Florianópolis, 2000.
[11] Y.K. Lee, C.S. Choi, Driving force for $\gamma \rightarrow \varepsilon$ martensitic transformation and stacking fault energy of γ in FeMn binary system, Metallurgical and Materials Transactions A 31A (2000) 355–360.
[12] W. Liu, et al., Cavitation erosion behavior of Cr–Mn–N stainless steels in comparison with 0Cr13Ni5Mo stainless steel, Wear 254 (2003) 713–722.
[13] J. Kim, et al., Effect of manganese on the cavitation erosion resistance of iron–chromium–carbon–silicon alloys for replacing cobalt-base stellite, Journal of Nuclear Materials 352 (2006) 85–89.
[14] P.D. Bilmes, et al., C.L. Characteristics and effects of austenite resulting from tempering of 13Cr–NiMo martensitic steel weld metals, Materials Characterization 46 (2001) 285–296.
[15] G. García-Atance Fatjó, et al., Experimental study and analytical model of the cavitation ring region with small diameter ultrasonic horn, Ultrason. Sonochem. (2010), doi:10.1016/j.ultsonch.2009.12.006.
[16] G.W. Stachowiak, A.W. Batchelor, Engineering Tribology, Elesevier, Amsterdam, 1993.
[17] E. Folkhard, Welding Metallurgy of Stainless Steels, Springer Verlag, 1988.
[18] Z. Xiaojun, L.A.J. Procopiak, N.C. Souza, A.S.C.M. d'Oliveira, Phase transformation during cavitation erosion of a Co stainless steel, Materials Science and Engineering A358 (2003) 199–204.